Crystal Structure of an Activated Variant of Small Heat Shock Protein Hsp16.5

Hassane S. Mchaourab,*,[†] Yi-Lun Lin,[†] and Benjamin W. Spiller*,[‡],[§]

[†]Department of Molecular Physiology and Biophysics, Vanderbilt University Medical Center, Tennessee 37232, United States
[‡]Department of Pharmacology, Vanderbilt University Medical Center, Tennessee 37232, United States
[§]Department of Pathology, Microbiology and Immunology, Vanderbilt University Medical Center, Tennessee 37232, United States

Ⓢ *Supporting Information*

ABSTRACT: How does the sequence of a single small heat shock protein (sHSP) assemble into oligomers of different sizes? To gain insight into the underlying structural mechanism, we determined the crystal structure of an engineered variant of *Methanocaldococcus jannaschii* Hsp16.5 wherein a 14 amino acid peptide from human heat shock protein 27 (Hsp27) was inserted at the junction of the N-terminal region and the α-crystallin domain. In response to this insertion, the oligomer shell expands from 24 to 48 subunits while maintaining octahedral symmetry. Oligomer

rearrangement does not alter the fold of the conserved α-crystallin domain nor does it disturb the interface holding the dimeric building block together. Rather, the flexible C-terminal tail of Hsp16.5 changes its orientation relative to the α-crystallin domain which enables alternative packing of dimers. This change in orientation preserves a peptide-in-groove interaction of the C-terminal tail with an adjacent β-sandwich, thereby holding the assembly together. The interior of the expanded oligomer, where substrates presumably bind, retains its predominantly nonpolar character relative to the outside surface. New large windows in the outer shell provide increased access to these substrate-binding regions, thus accounting for the higher affinity of this variant to substrates. Oligomer polydispersity regulates sHSPs chaperone activity *in vitro* and has been implicated in their physiological roles. The structural mechanism of Hsp16.5 oligomer flexibility revealed here, which is likely to be highly conserved across the sHSP superfamily, explains the relationship between oligomer expansion observed in disease-linked mutants and changes in chaperone activity.
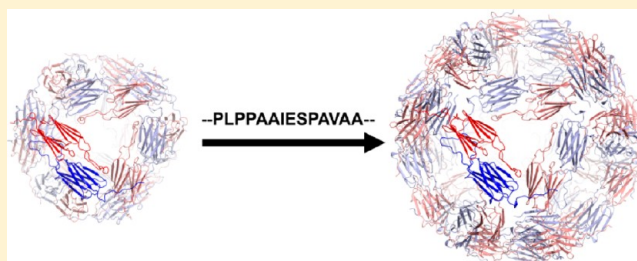
Cells face the continual challenge of preventing or reversing protein aggregation.[1] Driven by stress, mutations, and inefficient folding, the accumulation of stable aggregates is associated with a range of protein deposition maladies.[2,3] Five superfamilies of heat shock proteins function as molecular chaperones binding non-native states of proteins, thus providing a competing pathway for these toxic intermediates.[4] Among heat shock proteins, the ubiquitously expressed small heat shock proteins (sHSPs)[5−7] sequester unfolded or misfolded proteins without direct ATP hydrolysis. This function is exemplified by their ability to buffer rapid and persistent increases in aggregation-prone intermediates, thereby preventing futile refolding cycles by other HSPs.[8]

While mechanistic elements of sHSP chaperone activity appear to be conserved, the structural scaffold has undergone significant divergence.[6] Expressed as subunits of 12−42 kDa,[9] sHSPs assemble into large oligomers (12−40 subunits) with a remarkable spectrum of symmetries and size across the superfamily, ranging from ordered[10,11] to heterogeneous and dynamic ensembles of interconverting oligomers.[9,12−15] This architectural diversity stands in stark contrast to the conservation of tertiary and quaternary structures in other heat shock protein families such as Hsp60, -70, -90, and -100.

The property of forming multiple oligomers with dynamic assembly and disassembly, prevalent in metazoan sHSPs, has been linked to the regulation of substrate recognition and binding.[6,16−18] Disease-linked mutations in human sHSPs lead to changes in their polydisperisty, often inducing the formation of larger oligomers.[19−21]

An outstanding question in the chaperone field is how are sHSPs able to form a diverse group of oligomers using a single sequence. Sequence identity is highest in a 90−100 amino acid module referred to as the α-crystallin domain and considered the defining characteristic for membership in the superfamily.[9,22] This domain has a conserved core fold consisting of a 7-stranded β-sandwich.[10,11,14,23−25] Furthermore, dimers of the α-crystallin domain form the building blocks of sHSP oligomers. The C-terminal to α-crystallin domain is a stretch of 10−20 amino acids, the C-terminal tail or extension containing a conserved 4-residue stretch critical for oligomer assembly.[26] The most divergent region in size and sequence is the N-terminal extension which ranges from short amino acid

sequences to entire domains in human sHSPs.[9,27] Sequence similarity in this domain is only observed between closely related species.

In contrast to the wealth of biochemical data on sHSP chaperone activity, there is a dearth of high-resolution structures of their assemblies. Indeed, the extreme polydispersity of metazoan sHSP has frustrated crystallographic analysis, and structures of the native oligomer are limited to the ordered archeal *Methanocaldococcus jannaschii* Hsp16.5[10] and eukaryotic *Triticum aestivum* (wheat) Hsp16.9.[11] Although both Hsp16.5 and Hsp16.9 are built from similar dimers of the α-crystallin domain, the former assembles into a spherical oligomer of 24 subunits with octahedral symmetry while the Hsp16.9 oligomer consists of two stacked hexameric rings. The two structures provide an example of the interplay between the three sequence modules in determining higher order assemblies. A conserved motif in the C-terminal tail straps α-crystallin dimers through interaction with the edge of the α-crystallin domain β-sandwich. The different oligomer architectures of Hsp16.5 and Hsp16.9 arise from different orientations of the C-terminal tail relative to the α-crystallin domain.

Extension of these architectural principles to polydisperse sHSP oligomers is complicated by sequence divergence particularly the expansion of the N-terminal region. In polydisperse sHSP, the N-terminal domain plays an important role in stabilizing the assembly and conferring its dynamic properties. Truncation of this domain in α-crystallin and Hsp27 decreases the average oligomer size to dimers and tetramers and inhibits the phenomenon of subunit exchange.[24,28−31] Furthermore, phosphorylation of αB-crystallin and Hsp27 at sites in the N-terminal domain shifts the oligomer equilibrium toward monomers and dimers, respectively.[17,32] This shift is tightly coupled to substrate binding *in vitro*[17,33] and is physiologically important.[34,35] For instance, Hsp27 phosphorylation increases substrate affinity through the exposure of the otherwise buried N-terminal domain upon dissociation to a dimer. Hsp27 dissociation regulates its ability to rescue neuronal plasticity in tau transgenic mice.[35]

In contrast to α-crystallins and Hsp27, deletion of the entire N-terminal region of Hsp16.5 does not affect the overall size and symmetry of the oligomeric assembly.[36] Previous EPR and cryoEM analyses have shown that the construct consisting of the α-crystallin domain and C-terminal tail encodes all the interactions necessary to assemble the Hsp16.5 oligomer.[37] However, this region is functionally important and sequence modifications in the N-terminal region alter the size and order of the assembly. Shi et al. constructed Hsp16.5 variants that recapitulate aspects of mammalian sHSP oligomers such as size expansion and polydispersity.[38] A 14 amino acid peptide, referred to as P1, unique to Hsp27 was inserted into the N-terminal region of Hsp16.5. Deletion of P1 inhibits Hsp27 equilibrium dissociation to dimers by stabilizing its ensemble of large oligomers. When P1 was inserted at the junction of the N-terminal region and C-terminal domain of Hsp16.5 (this construct is referred to hereafter as Hsp16.5-P1), the oligomer size increased from 24 to 48 subunits. In contrast, P1 insertion in the middle of a helix in the N-terminal domain yielded an ensemble of polydisperse oligomers. Both constructs displayed higher affinity toward substrate, suggesting oligomer expansion is required for substrate binding.

To understand the molecular determinants that enable Hsp16.5 to form oligomeric shells of both 24 and 48 subunits and to inform molecular mechanisms for polydispersity in other

sHSPs, we determined the crystal structure of Hsp16.5-P1 at 2.7 Å resolution (Table 1, Figure S1). The structure of the 48

Table 1. Data Collection and Refinement Statistics[a]

data collection	
space group	*I*432
cell dimensions (Å)	
a, b, c (Å)	184.58
α, β, γ (deg)	90.00
resolution (Å)	2.7
R_{sym} (%)	4.3(60)
$I/\sigma I$	16.5(2.1)
completeness (%)[b]	98.9(94.4), 98.9(100)
redundancy	4.7(4.7)
refinement	
resolution range (Å)	50−2.7
no. of reflections	14 902
R_{factor} (%)	21.4
R_{free} (%)	23.7
total protein atoms	1791
total water molecules	10
RMSD	
bond lengths	0.009
bond angles	1.089
Ramachandran (%)	
favored	98.7
allowed	1.3
outliers	0
B-factors	
all	92
main chain	87
side chain	96
solvent	70

[a]Numbers in parentheses describe data in the highest resolution bin (2.79−2.70 Å). [b]For completeness, two sets of numbers are given. The first are completeness of data used in refinement (including the test set). The second are completeness from data reduction.

subunit octahedral shell reveals that oligomer expansion is mediated by reorientation of the C-terminal tail rather than changes in the α-crystallin dimer architecture, in agreement with predictions based on low-resolution cryoEM models.[38] Comparison with the WT Hsp16.5 structure reveals the molecular strategies used by sHSPs to form multiple oligomers. Changes in the N-terminal region are propagated to the C-terminal tail enabling alternative assemblies. Analysis of the structure rationalizes the increase in substrate affinity that has been reported to accompany oligomer expansion induced by disease-associated mutations.[19]

■ MATERIALS AND METHODS

Expression, Purification, Crystallization, and Data Collection. The construction of Hsp16.5-P1 was previously described.[38] Briefly, a sequence encoding human Hsp27 amino acids 57−70 (PLPPAAIESPAVAA) was inserted between residues 33 and 34 of Hsp16.5. Hsp16.5-P1 was expressed in *E. coli* BL21 (DE3) cells containing a pET20b+ derived plasmid.[38] Cell disruption was followed by addition of polyethylenimine to precipitate the DNA. Following high-speed centrifugation, the supernatant was loaded on an anion exchange chromatography column. Fractions containing Hsp16.5-P1 were pooled and further purified by gel filtration
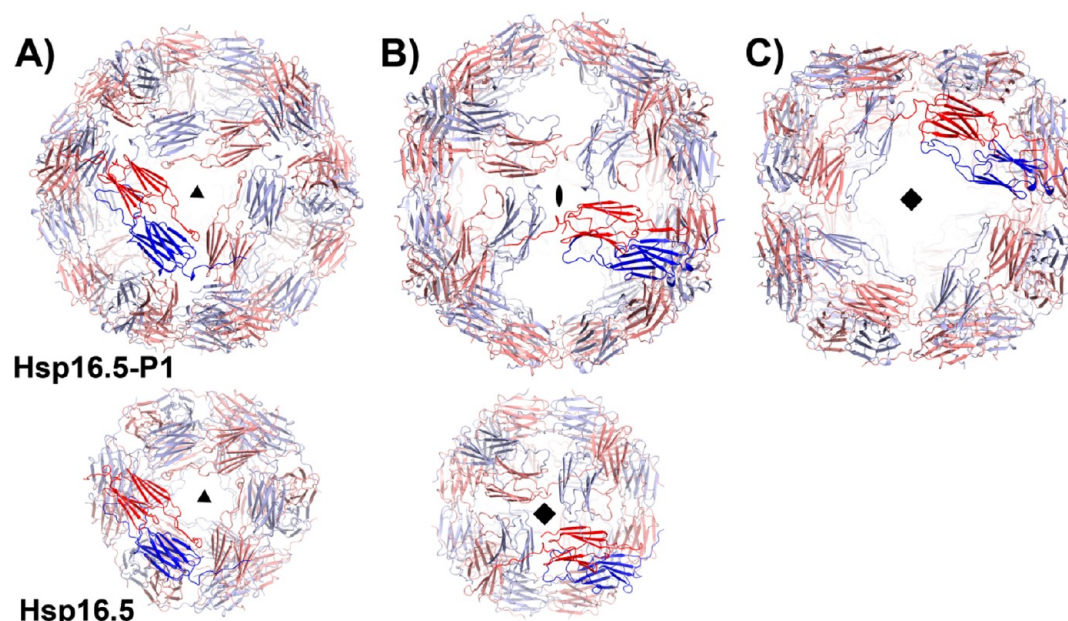
Figure 1. Views of Hsp16.5-P1 (upper row) and Hsp16.5-WT assemblies (PDB ID 1SHS, lower row) along their respective symmetry axes. The two shells are scaled to highlight the expansion of the P1 variant. Hsp16.5-P1 has (A) 3-fold, (B) 2-fold, and (C) 4-fold symmetry axes that relate dimers of the α-crystallin domain (blue and red). (B) By comparison, WT dimers of the α-crystallin domain are related by (A) 3-fold and (B) 4-fold symmetry.

in 20 mM HEPES pH 7.5 and 100 mM NaCl on a Superose 6 column.

Freshly purified protein was concentrated to 40 mg/mL before crystallization. Hanging drop vapor diffusion was used in crystallization trials. Crystals grew from 1.8 M $(NH_4)_2SO_4$, 20 mM Tris pH 8, and 10% glycerol at 25 °C. Diffraction data were collected at SER-CAT ID-22 at the Advanced Photon Source, Argonne National Laboratory, Argonne, IL.

Structure Determination and Analysis. Data were indexed, integrated, and scaled with HKL2000.[39] The space group of engineered Hsp16.5-P1 crystals was *I*432. There are two nonequivalent monomers forming a dimer in an asymmetric unit. Molecular replacement solutions were obtained using program PHASER[40] and were evaluated with omit maps calculated in CCP4[41] and displayed in COOT.[42] The structure was refined in CNS[43] and Phenix[44] and manually rebuilt into composite-omit maps (calculated initially in CNS and in later stages using Phenix) using COOT.[42] The overall R_{work} was 21.4% and R_{free} was 23.7%. RMS of bond lengths is 0.009 Å. RMS of bond angles is 1.1°. The final model contains 10 water molecules. There are zero Ramachandran outliers with 98.7% of residues in favored and 1.3% in allowed regions as determined by Phenix/Molprobity.[44,45] Data collection and refinement statistics are summarized in Table 1. Figures were produced in Pymol.[46] Solvent accessible surface areas were calculated in Pymol using a solvent sphere with a radius of 1.4 Å.[47,48]

■ RESULTS

Hsp16.5-P1 Oligomer Assembly. HSP16.5-P1 crystallized in the cubic space group *I*432 with 2 subunits in the crystallographic asymmetric unit. The octahedral shell is formed by crystallographic symmetry operators that allow formation of a spherical oligomer of 48 subunits, in agreement with the oligomer size determined by light scattering and low-resolution electron microscopy reconstructions.[38] Figure 1A−C

shows the views along the three windows of the outer shell capturing three symmetry axes that relate dimers of Hsp16.5-P1 (shown in dark red and blue). Thus, 24 Hsp16.5-P1 dimers are related by octahedral symmetry while the same symmetry operations relate 24 monomers in the WT.[10] Hsp16.5-P1 is expanded with an outer diameter of 163 Å compared to 115 Å for the WT. The expansion is manifested by a new large square opening in the outer shell (Figure 1C). The sides of this window consist of dimers of the α-crystallin domain related by 4-fold symmetry. The triangular 3-fold window is similar to that of the WT (Figure 1A). A 2-fold window between dimers replaces the 4-fold window relating monomers in the WT structure (Figure 1B).

In contrast to the α-crystallin domain and the C-terminal extension, the 32 amino acid N-terminal segment along with the 14 amino acid peptide insertion (P1) are crystallographically disordered and therefore not visible in the structure. Previous site-directed spin-labeling analysis assigned internal density observed in cryoEM images of the WT to the N-terminal region.[37] Although weak internal density, arising from the N-terminal segment and P1, was observed in the cryoEM model of Hsp16.5-P1, its poor reconstruction was interpreted as evidence of P1 flexibility.[38] The absence of density for this region, even in electron density maps calculated using only low-resolution terms (50−15 Å), indicates that these residues do not obey octahedral symmetry. The mechanism by which the inserted peptide P1 induces a gross oligomer reorganization is thus not directly observable. However, the structural consequences of this reorganization have herein been observed at 2.7 Å resolution, resulting in an atomic model describing a structural strategy used by sHSPs to expand the oligomer shell.

α-Crystallin Dimer. Despite the extensive reorganization of the oligomer as a result of P1 insertion, the overall fold of the α-crystallin domain is unchanged. Nine β-strands are arranged in two sheets forming a β-sandwich (Figure 2A). A structure-based alignment with Hsp27 (Figure S2) highlights the
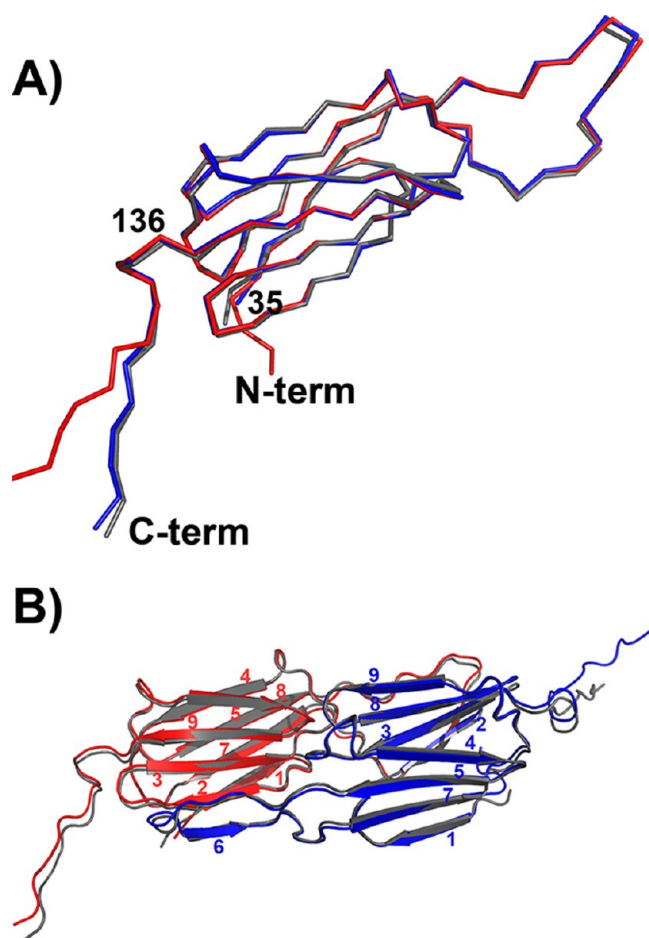
Figure 2. (A) Superposition of subunits from Hsp16.5-P1 (red and blue) and Hsp16.5-WT (gray) demonstrates that the α-crystallin domain fold is conserved and highlights the change in orientation of the C-terminal tail in one of the Hsp16.5-P1 subunits. (B) Ribbon diagram of the dimer from Hsp16.5-P1 (red and blue) superimposed on the dimer from Hsp16.5-WT (gray) shows that that oligomer expansion does not perturb the interface of the dimer involving stand swapping (strand 6) and extensive networks of contacts between loops.

conservation of the seven-strand core despite marginal sequence similarity between the archeal and human sHSPs. Superposition of the β-sandwich from Hsp16.5-WT with that of the P1 variant yielded a root-mean-square deviation of 0.3 Å for main-chain atoms of residues 45 to 148, demonstrating the similarity of the two structures. A long loop extends from the sandwich enabling a short β-strand (strand 6) to hydrogen bond to an edge strand (strand 2) of another α-crystallin domain to form a composite β-sheet (Figure 2B). In addition to strand swapping, the α-crystallin domain dimer in Hsp16.5-P1 is stabilized by extensive hydrophobic contacts, hydrogen bonds, and ionic interactions along loop regions that connect the two sheets of the two β-sandwiches. The dimer interface which buries ~3400 Å^2 of solvent accessible surface area is identical to that found in the WT assembly (Figure 2B). The β-sandwich and the loops at the dimer interface have the lowest B factors in the structure (Figure S3).

Thus, the expansion of the oligomer does not involve repacking at the interface of the dimer or changes in the relative orientations of dimer subunits. Instead, the two subunits in the Hsp16.5-P1 dimer are rendered structurally inequivalent by the

distinct orientation of the C-terminal tail relative to the β-sandwich. Figure 2B shows that while the β-sheet core of the α-crystallin domain is superimposable, the C-terminal tail of one of the two subunits in the dimeric building block of Hsp16.5-P1 undergoes a change of orientation relative to the β-sandwich. Whereas subunit A is overly similar to the WT structure, there is a clear displacement of the tail of subunit B. The change in orientation of this region is enabled by a reorientation at Ile140 such that there is an ~30° difference in the orientation of residues 141−147 between the two subunits (Figure 2A).

Similar dimer structures and octahedral symmetry of the assembly preserve the electrostatic contrast between the outside and inside of the sphere observed in the WT structure (Figure 3A,B).[10] The accessible surface on the inside is largely nonpolar, whereas the 3- and 4-fold windows on the surface are decorated by charged residues. This observation is consistent with recent cryoEM analysis demonstrating that T4 lysozyme binds to the inside of the Hsp16.5-P1 particle [Shi, J., Koteiche, H. A., Stewart, P. L., and Mchaourab, H. S.,
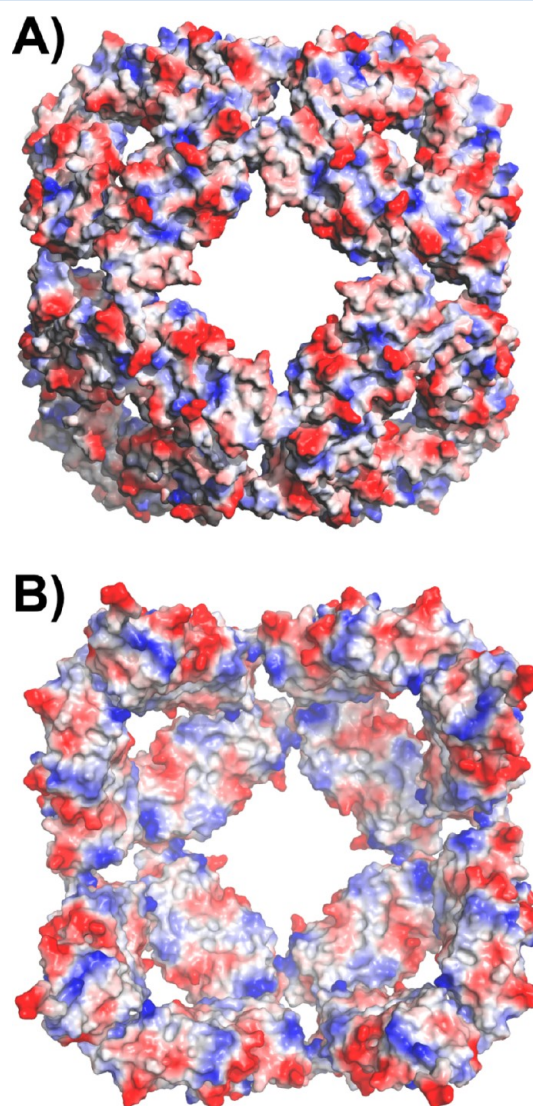

Figure 3. (A) Exterior and (B) interior of the Hsp16.5-P1 sphere viewed along the 4-fold symmetry axis and colored by residue polarity. The predominant nonpolar character of the internal surface provides plausible contact sites for bound substrates.
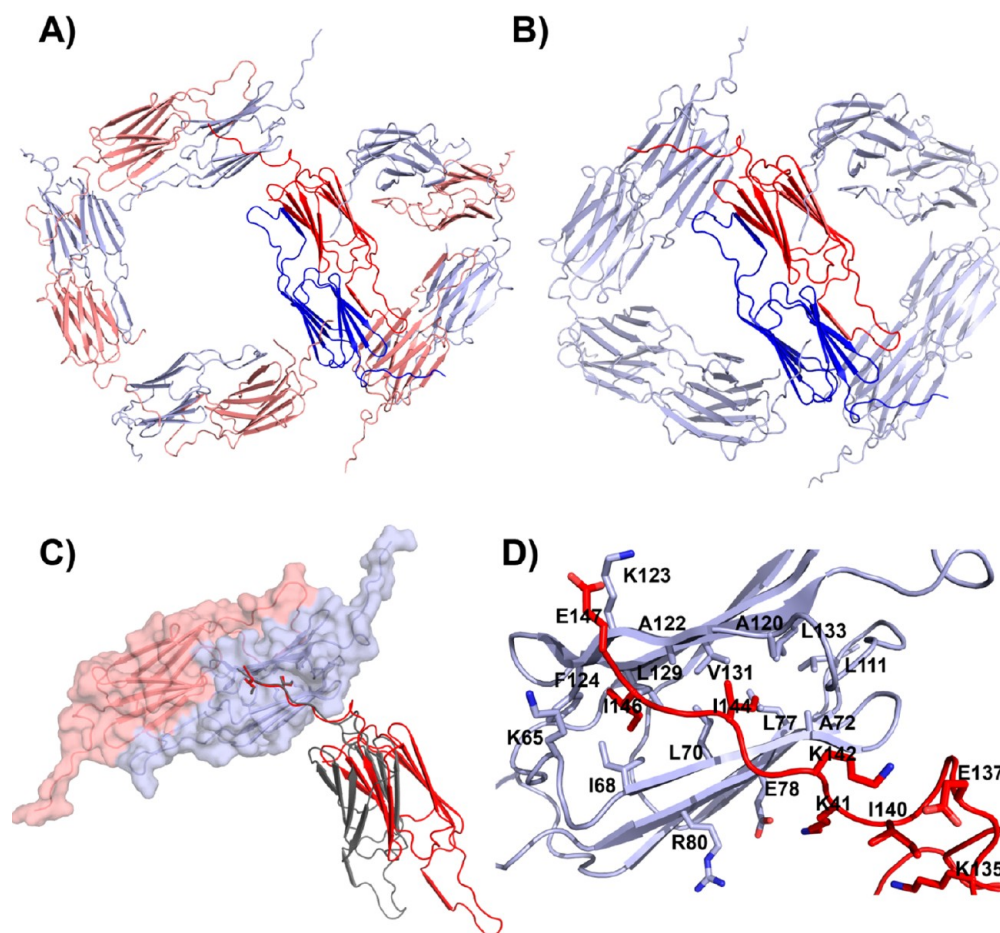
Figure 4. (A) Dimer packing around 3- and 4-fold windows of Hsp16.5-P1. The different angles between α-crystallin domain in the two windows are enabled by two distinct orientations of the C-terminal tail in the blue and red subunits. (B) By comparison, the angle between dimers is uniform in the WT assembly where a single orientation of the C-terminal tail is observed. (C) Peptide-in-groove interaction stabilizing contacts between subunits in the Hsp16.5-P1 (red and Hsp16.5-WT (gray). Note the change in relative orientation between the gray and red subunits. The gray orientation is seen in Hsp16.5-WT and in 3-fold window of Hsp16.5-P1. The red orientation is seen only in the 4-fold window of Hsp16.5-P1. (D) Close-up view of (C) showing the side chains stabilizing the peptide-in-groove interaction.

unpublished results] and supports a binding mode in which unfolded proteins can interact with the largely hydrophobic interior surface.

Two C-Terminal Tail Orientations Enable Distinct Dimer−Dimer Packing. To assemble the expanded Hsp16.5-P1 shell, the two subunits in a dimer, inequivalent by virtue of the C-terminal tail conformations, interact along 2-, 3-, and 4-fold symmetry interfaces. At the corner of the 3-fold window, the dimer−dimer interface is very similar to that of the WT (Figure 4A,B).[10] This interface has the least extensive contacts in the assembly burying ~400 Å^2 of solvent accessible surface area, whereas ~530 Å^2 is buried in the WT structure. In both instances, this interaction is stabilized by the C-terminal tail, which extends out and interacts with the hydrophobic groove at the edge of the neighboring β-sandwich. Ile 144 and Ile 146 from the C-terminal tail of one subunit make contacts with hydrophobic pockets on the edge of the β-sandwich of an adjacent subunit. Ile 144 is buried in a pocket formed by L70, L77, A72, L133, A120, V131, A122, and Ile 146 is buried in a pocket formed by F124, L129, A122, I68, L70 (Figure 4C,D). This peptide-in-groove interaction is quite extensive and buries ~1100 Å^2 of solvent-accessible surface area, allowing for flexibility at this interface. The conformation of the C-terminal

tail along the 3-fold window is identical to that observed in the WT subunit.

The large 4-fold window, which distinguishes the structure of Hsp16.5-P1, is assembled using the same dimer−dimer interactions observed at the corners of the 3-fold window. However, the angle between α-crystallin domain dimers is closer to 90°, whereas it is closer to 60° at the 3-fold window (Figure 4A). This interface highlights the significance of the assembly strategy utilized by sHSPs. While similar to the interfaces at the corners of the 3-fold window, the wider angle between α-crystallin domain dimers results in a complete loss of contacts between these domains. No buried surface area on the α-crystallin domain is associated with this interaction, and the hydrophobic peptide-in-groove interaction described in the previous paragraph (Figure 4C,D) suffices to stabilize this interface. The combination of the strong interaction between the C-terminal tail and the hydrophobic groove at the edge of the β-sandwich and the relatively weak interaction between adjacent α-crystallin domains gives these interfaces both stability and flexibility.

■ **DISCUSSION**

This paper reports the first structural insight into the basis of oligomer flexibility in a single sHSP. Oligomer polydispersity

has been reported for evolutionary distant sHSPs and is induced by an increase in temperature, disease-causing mutations, or substrate binding. Our findings reveal how sequence modifications in the N-terminal domain can remodel the overall assembly without altering the α-crystallin domain fold or the dimeric building block. Repacking of the N-terminal domain, here as a consequence of sequence insertion, is propagated to the C-terminal tail which can adopt two conformations compatible with a different assembly size built by the same symmetry elements. In addition to the 48-subunit assemblies reported here, Hsp16.5 can be induced to form heterogeneous ensembles of structures presumably mediated by the same elements of flexibility.[38] The linkage between shell size and C-terminal tail conformation uncovered by the structure of Hsp16.5-P1 illustrates how larger N-terminal domain sequences, characteristic of eukaryotic sHSP, can modulate the size and stability of the oligomeric assembly. Consistent with this notion, two different conformations of the C-terminal tail appear to be associated with different conformations of the N-terminal domain in Hsp16.9.[26] Furthermore, recent NMR and mass spectrometry based modeling of αB-crystallin invoked fluctuations of the C-terminal tail as a determinant of its oligomer polydispersity.[49]

The expansion of Hsp16.5-P1 provides insight into sHSP activation which is a critical element of their chaperone mechanism. There is a mounting body of evidence implicating sequences in the N-terminal regions of sHSPs in high affinity binding to client proteins.[7] Two models have been advanced to describe the basis of substrate recognition and binding. For the polydisperse and dynamic oligomers, substrate binding is mediated by a dimeric unit that is in equilibrium with the ensemble of large oligomers.[17] Dissociation to dimers exposes the N-terminal domain in an unstructured conformation.[50] In contrast, a dissociation-independent model,[51] proposed for ordered sHSPs, invokes conformational changes in the oligomer as the mechanism for access to the otherwise buried N-terminal domain. The Hsp16.5-P1 structure is the first direct view of how access to binding sites in the N-terminal domain can be accomplished without subunit dissociation. Indeed, Hsp16.5-P1 has an order of magnitude higher apparent affinity for substrates than does the WT.[38] Because assembly rearrangement does not alter the hydrophobic nature of the internal surface of the oligomer, the higher apparent substrate affinity of Hsp16.5-P1 likely arises from increased access enabled by the large windows in its shell.

Considering the binding capacity of sHSPs which can reach one subunit of equal molecular mass, loss of regulation of their interaction with client proteins can have deleterious consequences on proteostasis as evident from the association of sHSP point mutations with multiple inherited diseases in mouse models[52−54] and in humans.[55−58] Remarkably, many of these mutants have higher affinity to model substrates.[19,59] Consistent with the two activation mechanisms described above, these mutations either induce expansion of the oligomer or increase dissociation. For example, αA-crystallin mutant R116C,[20,60] which causes a dominant human cataract phenotype, and αB-crystallin R120G,[21] which is a dominant human mutation linked to cardiomyopathy, show increased average molecular mass. Determination of modes of sHSP oligomer flexibility is thus critical to understanding the molecular basis of these pathologies.

■ ASSOCIATED CONTENT

Ⓢ Supporting Information

Figures S1−S3. This material is available free of charge via the Internet at http://pubs.acs.org.

Accession Codes

The structure and data files have been deposited at the protein database with the accession code 4ELD.

■ AUTHOR INFORMATION

Corresponding Author

*Ph (615) 322-3307, Fax (615) 322-7236, e-mail hassane.mchaourab@vanderbilt.edu (H.S.M.); Ph (615) 322-6766, Fax (615) 343-6532, e-mail Benjamin.spiller@vanderbilt.edu (B.W.S.).

Notes

The authors declare no competing financial interest.

■ ACKNOWLEDGMENTS

■ ABBREVIATIONS

sHSP, small heat shock protein; Hsp16.5, *Methanocaldococcus jannaschii* heat shock protein 16.5; Hsp16.9, *Triticum aestivum* heat shock protein 16.9; Hsp27, heat shock protein 27; WT, wild-type.

■ REFERENCES

(1) Dobson, C. M. (2004) Principles of protein folding, misfolding and aggregation. *Semin. Cell Dev. Biol. 15*, 3−16.

(2) Gidalevitz, T., Kikis, E. A., and Morimoto, R. I. (2010) A cellular perspective on conformational disease: the role of genetic background and proteostasis networks. *Curr. Opin. Struct. Biol. 20*, 23−32.

(3) Balch, W. E., Morimoto, R. I., Dillin, A., and Kelly, J. W. (2008) Adapting proteostasis for disease intervention. *Science 319*, 916−919.

(4) Hartl, F. U., Bracher, A., and Hayer-Hartl, M. (2011) Molecular chaperones in protein folding and proteostasis. *Nature 475*, 324−332.

(5) Haslbeck, M., Franzmann, T., Weinfurtner, D., and Buchner, J. (2005) Some like it hot: the structure and function of small heat-shock proteins. *Nat. Struct. Mol. Biol. 12*, 842−846.

(6) McHaourab, H. S., Godar, J. A., and Stewart, P. L. (2009) Structure and mechanism of protein stability sensors: chaperone activity of small heat shock proteins. *Biochemistry 48*, 3828−3837.

(7) Basha, E., O'Neill, H., and Vierling, E. (2012) Small heat shock proteins and α-crystallins: dynamic proteins with flexible functions. *Trends Biochem. Sci. 37*, 106−117.

(8) Lee, G. J., Roseman, A. M., Saibil, H. R., and Vierling, E. (1997) A small heat shock protein stably binds heat-denatured model substrates and can maintain a substrate in a folding-competent state. *EMBO J. 16*, 659−671.

(9) de Jong, W. W., Caspers, G. J., and Leunissen, J. A. (1998) Genealogy of the α-Crystallin--small heat-shock protein superfamily. *Int. J. Biol. Macromol. 22*, 151−162.

(10) Kim, K. K., Kim, R., and Kim, S. H. (1998) Crystal structure of a small heat-shock protein. *Nature 394*, 595−599.

(11) van Montfort, R. L., Basha, E., Friedrich, K. L., Slingsby, C., and Vierling, E. (2001) Crystal structure and assembly of a eukaryotic small heat shock protein. *Nat. Struct. Biol. 8*, 1025−1030.

(12) Haley, D. A., Bova, M. P., Huang, Q. L., Mchaourab, H. S., and Stewart, P. L. (2000) Small heat-shock protein structures reveal a

continuum from symmetric to variable assemblies. *J. Mol. Biol. 298*, 261−272.

(13) Haslbeck, M., Walke, S., Stromer, T., Ehrnsperger, M., White, H. E., Chen, S., Saibil, H. R., and Buchner, J. (1999) Hsp26: a temperature-regulated chaperone. *EMBO J. 18*, 6744−6751.

(14) Jehle, S., van Rossum, B., Stout, J. R., Noguchi, S. M., Falber, K., Rehbein, K., Oschkinat, H., Klevit, R. E., and Rajagopal, P. (2009) alphaB-Crystallin: a hybrid solid-state/solution-state NMR investigation reveals structural aspects of the heterogeneous oligomer. *J. Mol. Biol. 385*, 1481−1497.

(15) Haley, D. A., Horwitz, J., and Stewart, P. L. (1998) The small heat-shock protein, αB-Crystallin, has a variable quaternary structure. *J. Mol. Biol. 277*, 27−35.

(16) Koteiche, H. A., and McHaourab, H. S. (2003) Mechanism of chaperone function in small heat-shock proteins. Phosphorylation-induced activation of two-mode binding in alphaB-Crystallin. *J. Biol. Chem. 278*, 10361−10367.

(17) Shashidharamurthy, R., Koteiche, H. A., Dong, J., and McHaourab, H. S. (2005) Mechanism of chaperone function in small heat shock proteins: dissociation of the HSP27 oligomer is required for recognition and binding of destabilized T4 lysozyme. *J. Biol. Chem. 280*, 5281−5289.

(18) Giese, K. C., and Vierling, E. (2002) Changes in oligomerization are essential for the chaperone activity of a small heat shock protein in vivo and in vitro. *J. Biol. Chem. 277*, 46310−46318.

(19) Koteiche, H. A., and McHaourab, H. S. (2006) Mechanism of a Hereditary Cataract Phenotype: Mutations in αA-Crystallin activate substrate binding. *J. Biol. Chem. 281*, 14273−14279.

(20) Cobb, B. A., and Petrash, J. M. (2000) Structural and functional changes in the αA-Crystallin R116C mutant in hereditary cataracts. *Biochemistry 39*, 15791−15798.

(21) Bova, M. P., Yaron, O., Huang, Q., Ding, L., Haley, D. A., Stewart, P. L., and Horwitz, J. (1999) Mutation R120G in αB-Crystallin, which is linked to a desmin-related myopathy, results in an irregular structure and defective chaperone-like function. *Proc. Natl. Acad. Sci. U. S. A. 96*, 6137−6142.

(22) Poulain, P., Gelly, J. C., and Flatters, D. (2010) Detection and architecture of small heat shock protein monomers. *PLoS One 5*, e9990.

(23) Laganowsky, A., Benesch, J. L. P., Landau, M., Ding, L., Sawaya, M. R., Cascio, D., Huang, Q., Robinson, C. V., Horwitz, J., and Eisenberg, D. (2010) Crystal structures of truncated alphaA and alphaB crystallins reveal structural mechanisms of polydispersity important for eye lens function. *Protein Sci. 19*, 1031−1043.

(24) Bagneris, C., Bateman, O. A., Naylor, C. E., Cronin, N., Boelens, W. C., Keep, N. H., and Slingsby, C. (2009) Crystal Structures of α-Crystallin Domain Dimers of αB-Crystallin and Hsp20. *J. Mol. Biol. 392*, 1242−1252.

(25) Koteiche, H. A., and Mchaourab, H. S. (1999) Folding pattern of the α-Crystallin domain in αA-Crystallin determined by site-directed spin labeling. *J. Mol. Biol. 294*, 561−577.

(26) Van Montfort, R., Slingsby, C., and Vierling, E. (2001) Structure and function of the small heat shock protein/alpha-Crystallin family of molecular chaperones. *Adv. Protein Chem. 59*, 105−156.

(27) Jehle, S., Vollmar, B. S., Bardiaux, B., Dove, K. K., Rajagopal, P., Gonen, T., Oschkinat, H., and Klevit, R. E. (2011) N-terminal domain of alphaB-Crystallin provides a conformational switch for multimerization and structural heterogeneity. *Proc. Natl. Acad. Sci. U. S. A. 108*, 6409−6414.

(28) Baranova, E. V., Weeks, S. D., Beelen, S., Bukach, O. V., Gusev, N. B., and Strelkov, S. V. (2011) Three-Dimensional Structure of α-Crystallin Domain Dimers of Human Small Heat Shock Proteins HSPB1 and HSPB6. *J. Mol. Biol. 411*, 110−122.

(29) Bova, M. P., Horwitz, J., and Fung, B. K. (1997) Subunit exchange of αA-Crystallin. *J. Biol. Chem. 272*, 29511−29517.

(30) Bova, M. P., Mchaourab, H. S., Han, Y., and Fung, B. K. (2000) Subunit exchange of small heat shock proteins. Analysis of oligomer formation of αA-Crystallin and Hsp27 by fluorescence resonance energy transfer and site-directed truncations. *J. Biol. Chem. 275*, 1035−1042.

(31) Berengian, A. R., Parfenova, M., and Mchaourab, H. S. (1999) Site-directed spin labeling study of subunit interactions in the α-Crystallin domain of small heat-shock proteins. Comparison of the oligomer symmetry in αA-Crystallin, HSP 27, and HSP 16.3. *J. Biol. Chem. 274*, 6305−6314.

(32) Aquilina, J. A., Benesch, J. L., Ding, L. L., Yaron, O., Horwitz, J., and Robinson, C. V. (2004) Phosphorylation of alphaB-Crystallin alters chaperone function through loss of dimeric substructure. *J. Biol. Chem. 279*, 28675−28680.

(33) Sathish, H. A., Stein, R. A., Yang, G., and Mchaourab, H. S. (2003) Mechanism of chaperone function in small heat-shock proteins. Fluorescence studies of the conformations of T4 lysozyme bound to alphaB-Crystallin. *J. Biol. Chem. 278*, 44214−44221.

(34) Rogalla, T., Ehrnsperger, M., Preville, X., Kotlyarov, A., Lutsch, G., Ducasse, C., Paul, C., Wieske, M., Arrigo, A. P., Buchner, J., and Gaestel, M. (1999) Regulation of Hsp27 oligomerization, chaperone function, and protective activity against oxidative stress/tumor necrosis factor alpha by phosphorylation. *J. Biol. Chem. 274*, 18947−18956.

(35) Abisambra, J. F., Blair, L. J., Hill, S. E., Jones, J. R, Kraft, C., Rogers, J., Koren, J., Jinwal, U. K, Lawson, L., Johnson, A. G., Wilcock, D., O'Leary, J. C., Jansen-West, K., Muschol, M., Golde, T. E., Weeber, E. J., Banko, J., and Dickey, C. A. (2010) Phosphorylation Dynamics Regulate Hsp27-Mediated Rescue of Neuronal Plasticity Deficits in Tau Transgenic Mice. *J. Neurosci. 30*, 15374−15382.

(36) Koteiche, H. A., and McHaourab, H. S. (2002) The determinants of the oligomeric structure in Hsp16.5 are encoded in the alpha-Crystallin domain. *FEBS Lett. 519*, 16−22.

(37) Koteiche, H. A., Chiu, S., Majdoch, R. L., Stewart, P. L., and McHaourab, H. S. (2005) Atomic models by cryo-EM and site-directed spin labeling: application to the N-terminal region of Hsp16.5. *Structure 13*, 1165−1171.

(38) Shi, J., Koteiche, H. A., Mchaourab, H. S., and Stewart, P. L. (2006) Cryoelectron Microscopy and EPR Analysis of Engineered Symmetric and Polydisperse Hsp16.5 Assemblies Reveals Determinants of Polydispersity and Substrate Binding. *J. Biol. Chem. 281*, 40420−40428.

(39) Otwinowski, Z., and Minor, W. (1997) Processing of X-ray Diffraction Data Collected in Oscillation Mode. *Methods Enzymol. 276A*, 307−326.

(40) McCoy, A. J., Grosse-Kunstleve, R. W., Storoni, L. C., and Read, R. J. (2005) Likelihood-enhanced fast translation functions. *Acta Crystallogr., Sect. D: Biol. Crystallogr. 61*, 458−464.

(41) Bailey, S. (1994) The CCP4 Suite - Programs for Protein Crystallography. *Acta Crystallogr., Sect. D: Biol. Crystallogr. 61*, 458−464.

(42) Emsley, P., and Cowtan, K. (2004) Coot: model-building tools for molecular graphics. *Acta Crystallogr., Sect. D: Biol. Crystallogr. 60*, 2126−2132.

(43) Brunger, A. T., Adams, P. D., Clore, G. M., DeLano, W. L., Gros, P., Grosse-Kunstleve, R. W., Jiang, J. S., Kuszewski, J., Nilges, M., Pannu, N. S., Read, R. J., Rice, L. M., Simonson, T., and Warren, G. L. (1998) Crystallography & NMR system: A new software suite for macromolecular structure determination. *Acta Crystallogr., Sect. D: Biol. Crystallogr. 54*, 905−921.

(44) Adams, P. D., Grosse-Kunstleve, R. W., Hung, L. W., Ioerger, T. R., McCoy, A. J., Moriarty, N. W., Read, R. J., Sacchettini, J. C., Sauter, N. K., and Terwilliger, T. C. (2002) PHENIX: building new software for automated crystallographic structure determination. *Acta Crystallogr., Sect. D: Biol. Crystallogr. 58*, 1948−1954.

(45) Davis, I. W., Leaver-Fay, A., Chen, V. B., Block, J. N., Kapral, G. J., Wang, X., Murray, L. W., Arendall, W. B., III, Snoeyink, J., Richardson, J. S., and Richardson, D. C. (2007) MolProbity: all-atom contacts and structure validation for proteins and nucleic acids. *Nucleic Acids Res. 35*, W375−383.

(46) DeLano, W. L. (2002) *The PyMOL Molecular Graphics System*, DeLano Scientific, San Carlos, CA.

(47) Connolly, M. L. (1983) Solvent-accessible surfaces of proteins and nucleic acids. *Science 221*, 709−713.

(48) Lee, B., and Richards, F. M. (1971) The interpretation of protein structures: estimation of static accessibility. *J. Mol. Biol. 55*, 379−400.

(49) Baldwin, A. J., Lioe, H., Hilton, G. R., Baker, L. A., Rubinstein, J. L., Kay, L. E., and Benesch, J. L. (2011) The polydispersity of alphaB-Crystallin is rationalized by an interconverting polyhedral architecture. *Structure 19*, 1855−1863.

(50) McDonald, E. T., Bortolus, M., Koteiche, H. A., and Mchaourab, H. S. (2012) Sequence, structure, and dynamic determinants of Hsp27 (HspB1) equilibrium dissociation are encoded by the N-terminal domain. *Biochemistry 51*, 1257−1268.

(51) Franzmann, T. M., Wuhr, M., Richter, K., Walter, S., Buchner, J., Franzmann, T. M., Wuhr, M., Richter, K., Walter, S., and Buchner, J. (2005) The activation mechanism of Hsp26 does not require dissociation of the oligomer. *J. Mol. Biol. 350*, 1083−1093.

(52) Hsu, C.-D., Kymes, S., and Petrash, J. M. (2006) A transgenic mouse model for human autosomal dominant cataract. *Invest. Ophthalmol. Visual Sci. 47*, 2036−2044.

(53) Xi, J. H., Bai, F., Gross, J., Townsend, R. R., Menko, A. S., Andley, U. P., Xi, J.-h., Bai, F., Gross, J., Townsend, R. R., Menko, A. S., and Andley, U. P. (2008) Mechanism of small heat shock protein function in vivo: a knock-in mouse model demonstrates that the R49C mutation in alpha A-Crystallin enhances protein insolubility and cell death. *J. Biol. Chem. 283*, 5801−5814.

(54) Wang, X., Osinska, H., Klevitsky, R., Gerdes, A. M., Nieman, M., Lorenz, J., Hewett, T., and Robbins, J. (2001) Expression of R120G-alphaB-Crystallin causes aberrant desmin and alphaB-Crystallin aggregation and cardiomyopathy in mice.[comment]. *Circ. Res. 89*, 84−91.

(55) Graw, J., Loster, J., Soewarto, D., Fuchs, H., Meyer, B., Reis, A., Wolf, E., Balling, R., and Hrabe de Angelis, M. (2001) Characterization of a new, dominant V124E mutation in the mouse alphaA-Crystallin-encoding gene. *Invest. Ophthalmol. Visual Sci. 42*, 2909−2915.

(56) Litt, M., Kramer, P., LaMorticella, D. M., Murphey, W., Lovrien, E. W., and Weleber, R. G. (1998) Autosomal dominant congenital cataract associated with a missense mutation in the human α Crystallin gene CRYAA. *Hum. Mol. Genet. 7*, 471−474.

(57) Mackay, D. S., Boskovska, O. B., Knopf, H. L. S., Lampi, K. J., and Shiels, A. (2002) A nonsense mutation in CRYBB1 associated with autosomal dominant cataract linked to human chromosome 22q. *Am. J. Hum. Genet. 71*, 1216−1221.

(58) Vicart, P., Caron, A., Guicheney, P., Li, Z., Prevost, M. C., Faure, A., Chateau, D., Chapon, F., Tome, F., Dupret, J. M., Paulin, D., and Fardeau, M. (1998) A missense mutation in the αB-Crystallin chaperone gene causes a desmin-related myopathy. *Nat. Genet. 20*, 92−95.

(59) Kumar, M. S., Koteiche, H. A., Claxton, D. P., and McHaourab, H. S. (2009) Disulfide cross-links in the interaction of a cataract-linked alphaA-Crystallin mutant with betaB1-Crystallin. *FEBS Lett. 583*, 175−179.

(60) Berengian, A. R., Bova, M. P., and Mchaourab, H. S. (1997) Structure and function of the conserved domain in αA-Crystallin. Site-directed spin labeling identifies a β-strand located near a subunit interface. *Biochemistry 36*, 9951−9957.